Molecular Cell, Volume *57*

Supplemental Information

Molecular Basis for SMC Rod Formation and Its Dissolution upon DNA Binding

Young-Min Soh, Frank Bürmann, Ho-Chul Shin, Takashi Oda, Kyeong Sik Jin, Christopher P. Toseland, Cheolhee Kim, Hansol Lee, Soo Jin Kim, Min-Seok Kong, Marie-Laure Durand-Diebold, Yeon-Gil Kim, Ho Min Kim, Nam Ki Lee, Mamoru Sato, Byung-Ha Oh, and Stephan Gruber

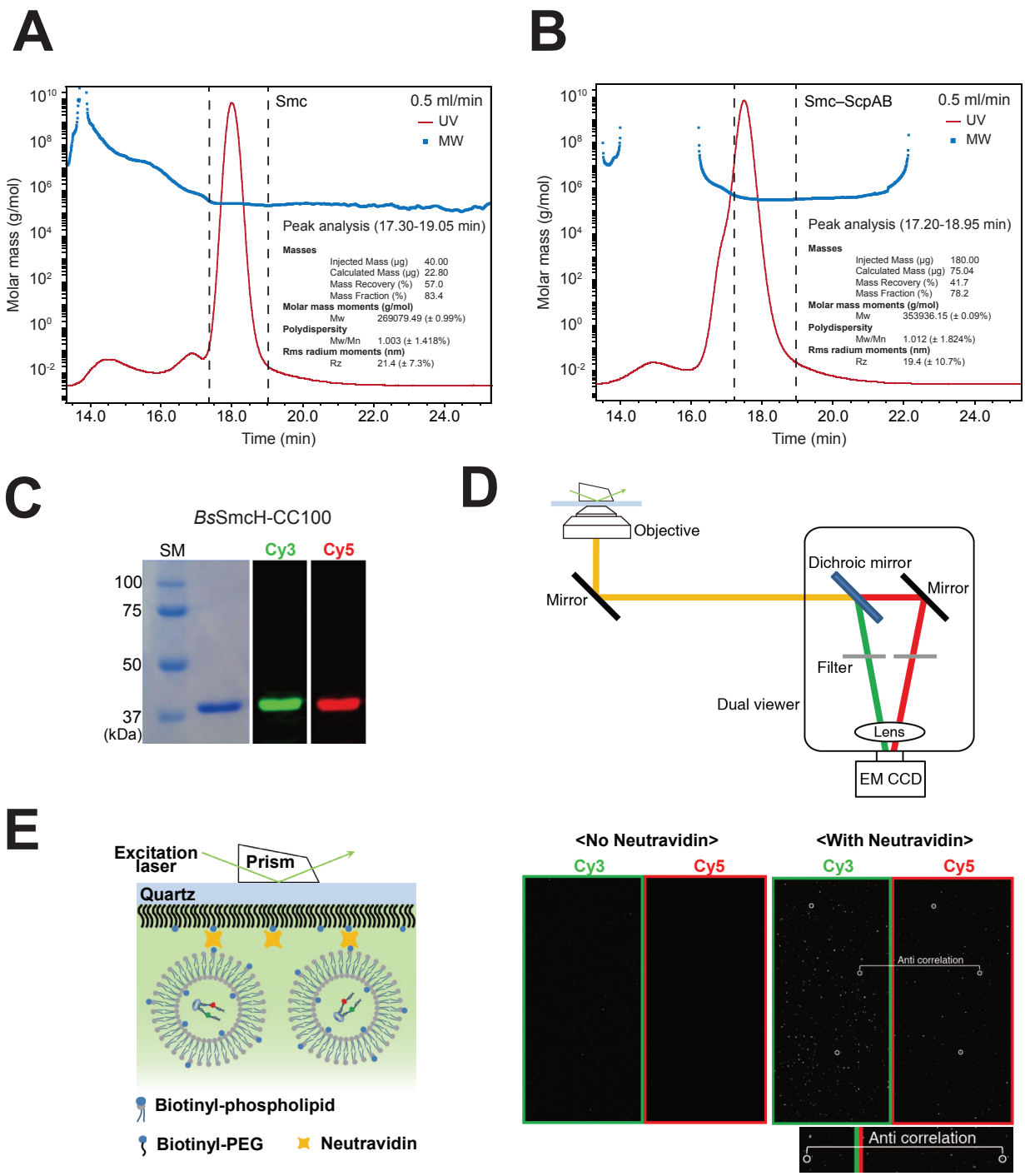

Figure S1

(Related to Figure 1)

Figure S1. SEC-MALS and FRET analysis of *Bs* Smc–ScpAB. Related to Figure 1.
(A) Purified fractions of *Bs* Smc were analyzed by size exclusion chromatography (Superdex 200 Increase 5/150) coupled to a multi angle light scattering detector (Wyatt Dawn TREOS-II). Molar mass (in g/mol) is plotted against the elution time from the size exclusion column (in min). The *Bs* Smc protein eluted from the size exclusion column as single peak at 18 min with an estimated molar mass of 269 kg/mol, which is consistent with it being a dimer (calculated molar mass: 271 kg/mol). Mw, weight-average molar mass; Mn, number-average molar mass.
(B) Same as in (A) with *Bs* Smc–ScpAB. The molar mass was calculated for the elution of the main peak between 17.2 and 18.95 min giving an estimate of 354 kg/mol, which is close to the calculated molar mass of a Smc_2–$ScpA_1$–$ScpB_2$ complex (345 kg/mol). In addition to this main peak a minor species eluted slightly earlier from the column.
(C) Cy3 and Cy5 labeling of *Bs*SmcH-CC100. The fluorescent band on a denaturing acrylamide gel confirms dual dye labeling. SM, size markers.
(D) Schematic drawing of the TIRF-FRET setup.
(E) Confirming vesicle immobilization. The immobilization strategy is shown in the left panel. Fluorescent signals (detecting Cy3 or Cy5 emission) in the presence of neutravidin confirmed immobilization of the vesicles containing dye-labeled *Bs*SmcH-CC100 (right panel). A vesicle containing a dye-labeled *Bs*SmcH-CC100 molecule appears as a single dot. The Cy3-Cy5 dimer exhibits both Cy3 and Cy5 signals as indicated by the circles. Because of FRET, the fluorescent signals of Cy3 and Cy5 are anti-correlated.
(F) FRET signals from single molecules were traced as a time course, and a representative one is shown. A high FRET state was maintained until the donor dye Cy3 was photobleached.
(G) FRET histogram of encapsulated *Bs*SmcH-CC100. A total of 123 time traces were analyzed that exhibited both donor and acceptor signals with single-step photobleaching.

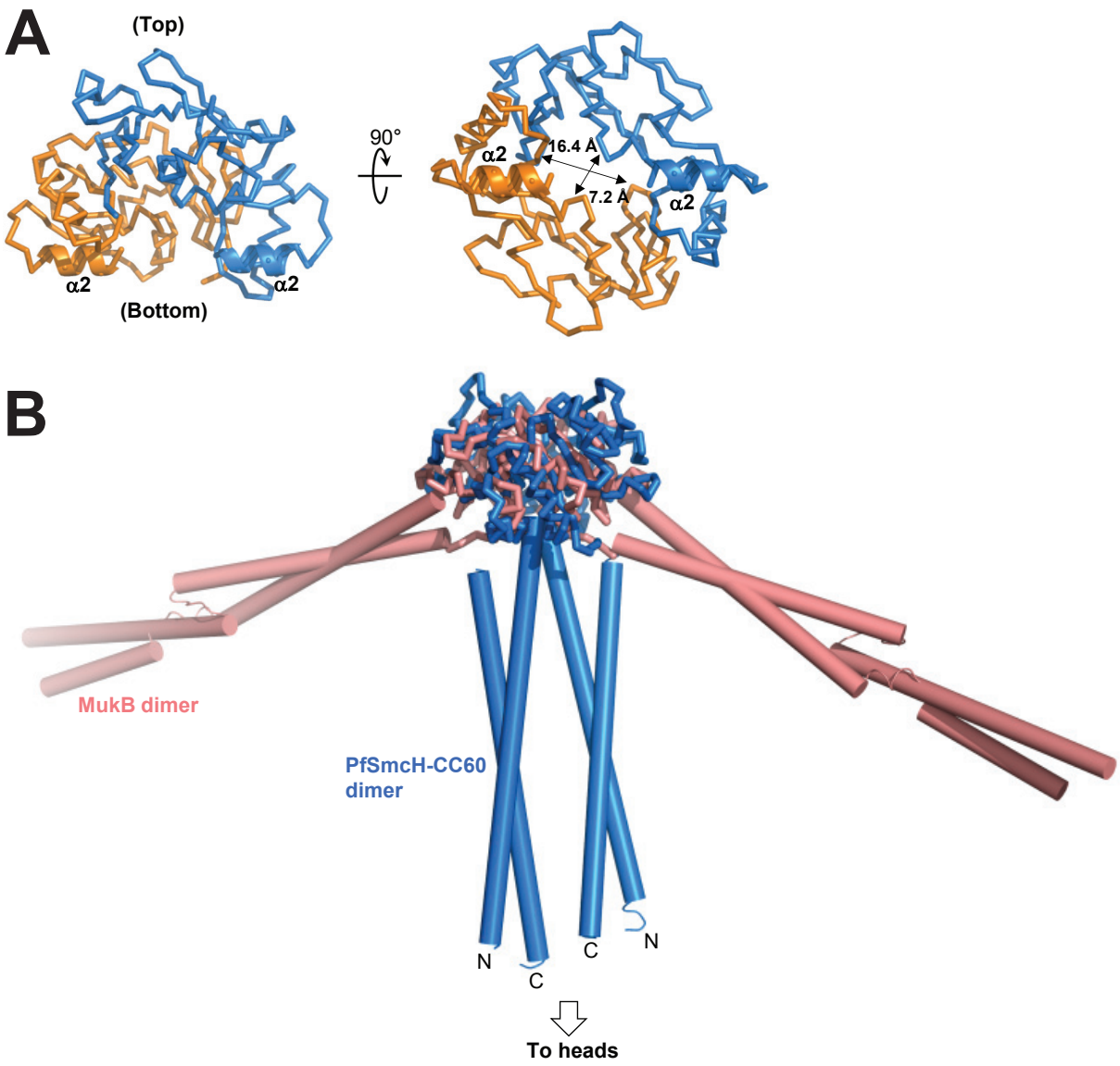

Figure S2

(Related to Figure 2)

Figure S2. Structural features of *Pf*SmcH-CC60. Related to Figure 2.

(A) The toroidal structure of the hinge domain homodimer. The coiled coils are omitted for clarity. A side and a top view are displayed on the left and right panel, respectively.

(B) Structural superposition of *Pf*SmcH-CC60 with a MukB hinge structure with long coiled coils (PDB entry: 3IBP).

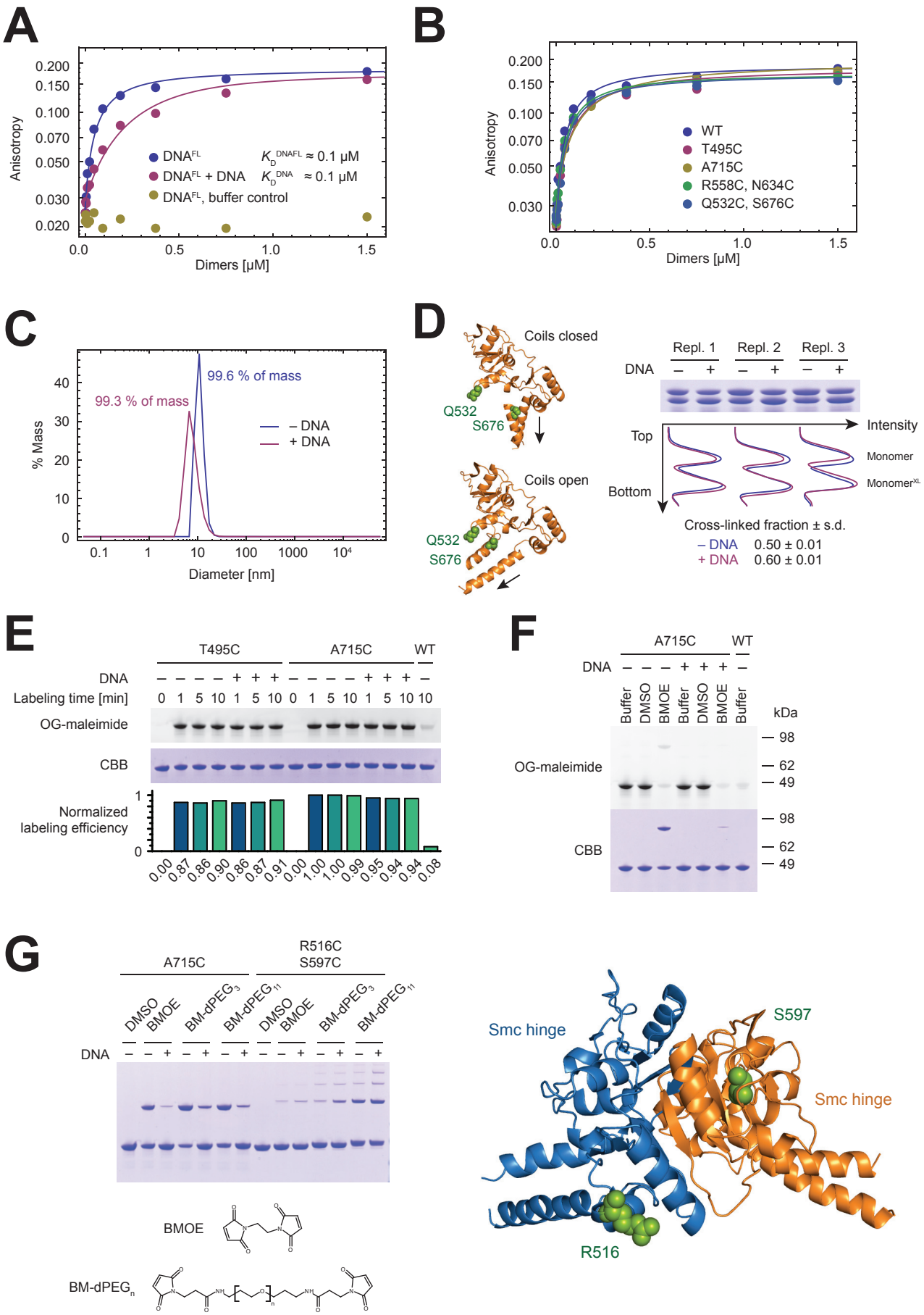

Figure S3

(Related to Figure 4)

Figure S3. Structural transition of the hinge-proximal coiled coil. Related to Figure 4.
(A) *Bs*SmcH-CC100 binds unlabeled DNA with similar affinity as fluorescein labeled DNA. Fluorescence anisotropy of 50 nM labeled double-stranded DNA (DNA^{FL}) was measured in the presence of 500 nM unlabeled DNA used for cross-linking experiments. Conditions were identical to those used for cross-linking experiments. Data were fitted with a competition model using K_D^{DNAFL} = 0.1 µM as a fixed parameter.
(B) DNA binding of *Bs*SmcH-C100 variants used in Fig. 4C. Buffer conditions were identical to those used for cross-linking experiments.
(C) *Bs*SmcH-CC100 forms defined complexes with DNA. Dynamic light scattering analysis of 6.5 µM protein in the presence or absence of 20 µM DNA under the same buffer conditions used for cross-linking experiments. Please note that scattering of free DNA is negligible.
(D) Structural transition at the coils/hinge interface. A model of *B. subtilis* Smc hinge conformations based on the *T. maritima* and *P. furiosus* structures predicts decreasing distance of Q532 and S676 residues upon coils opening (left panel). BMOE cross-linking analysis of *Bs*SmcH-CC100(Q532C, S676C) in the presence or absence of DNA (right panel). Bands were quantified by fitting densitograms (bottom right panel) with the sum of two skewed gaussians similar to the method of (Mitov et al., 2009).
(E) Cysteines in the *Bs*SmcH-CC100 coiled coil are reactive toward Oregon-Green maleimide in the presence of DNA. Labeling reactions were quenched at different time points and analysed by in-gel fluorescence and coomassie staining (CBB).
(F) A715C in the *Bs*SmcH-CC100 coiled coil is reactive toward BMOE in the presence of DNA. Cross-linking reactions were done as in Fig. 4C, except that an additional 1 min labeling step with Oregon-Green maleimide was included before quenching with 2-mercaptoethanol. CBB, coomassie brilliant blue.
(G) Cross-linking of *Bs*SmcH-CC100 cysteines with long cross-linkers. Predicted positions of R516 and S597 are shown in the right panel.

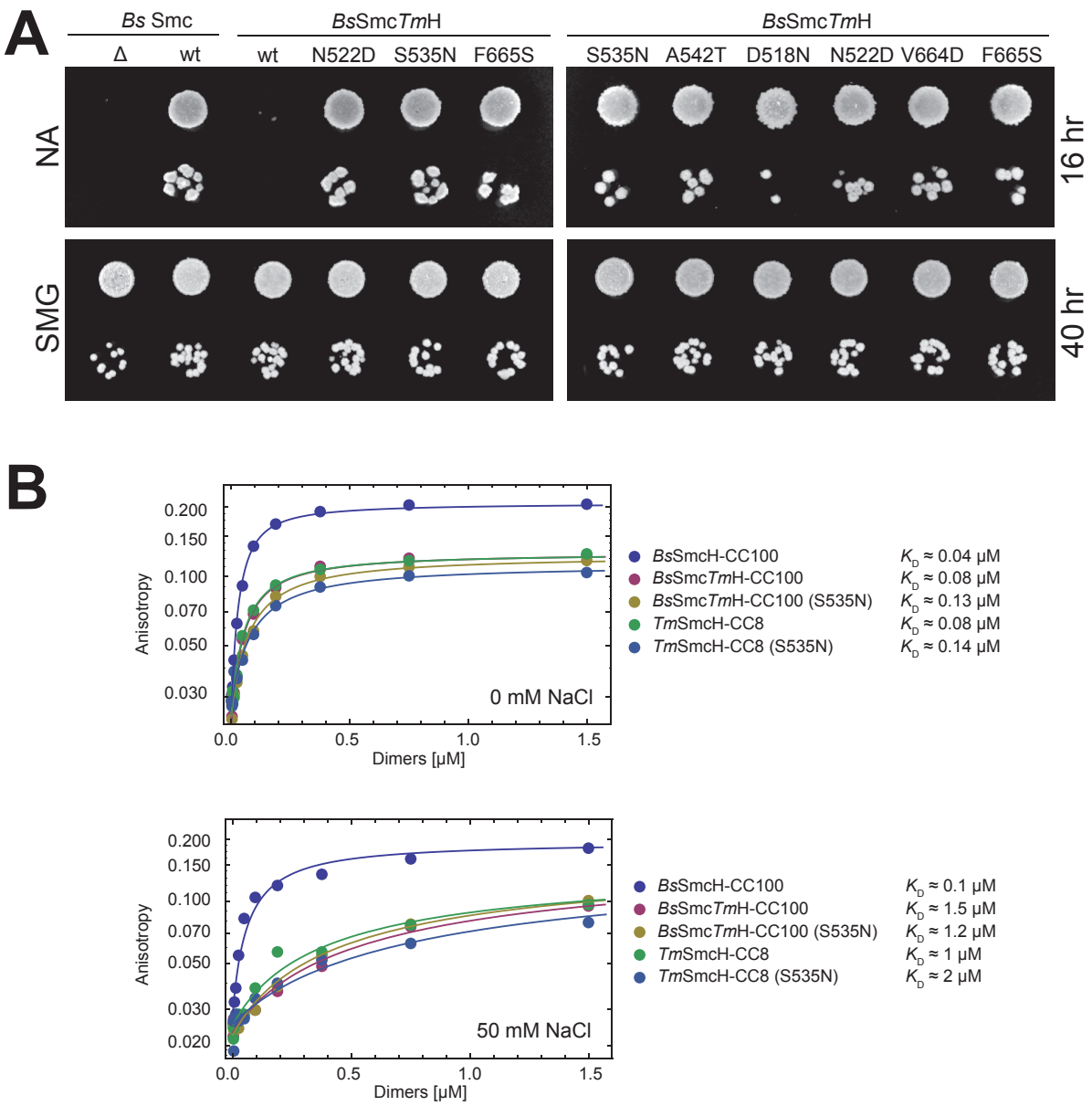

Figure S4

(Related to Figure 5)

Figure S4. Colony formation of *Bs* strains harboring chimeric Smc proteins. Related to Figure 5.

(A) Overnight cultures of strains (BSG1001, BSG1007, BSG1363, BSG1365-1368, BSG1966 and BSG1970) were serially diluted and spotted on nutrient agar (NA) or defined medium agar (SMG) and grown for 16 and 40 hr, respectively, at 37°C. Top left image is identical to figure panel 5A.

(B) DNA binding of *Bs*SmcH*Tm*H-CC100 chimeric constructs and *Tm*SmcH-CC8 hinges in buffer containing 0 mM NaCl or 50 mM NaCl. Former proteins contained C437S and A715C mutations.

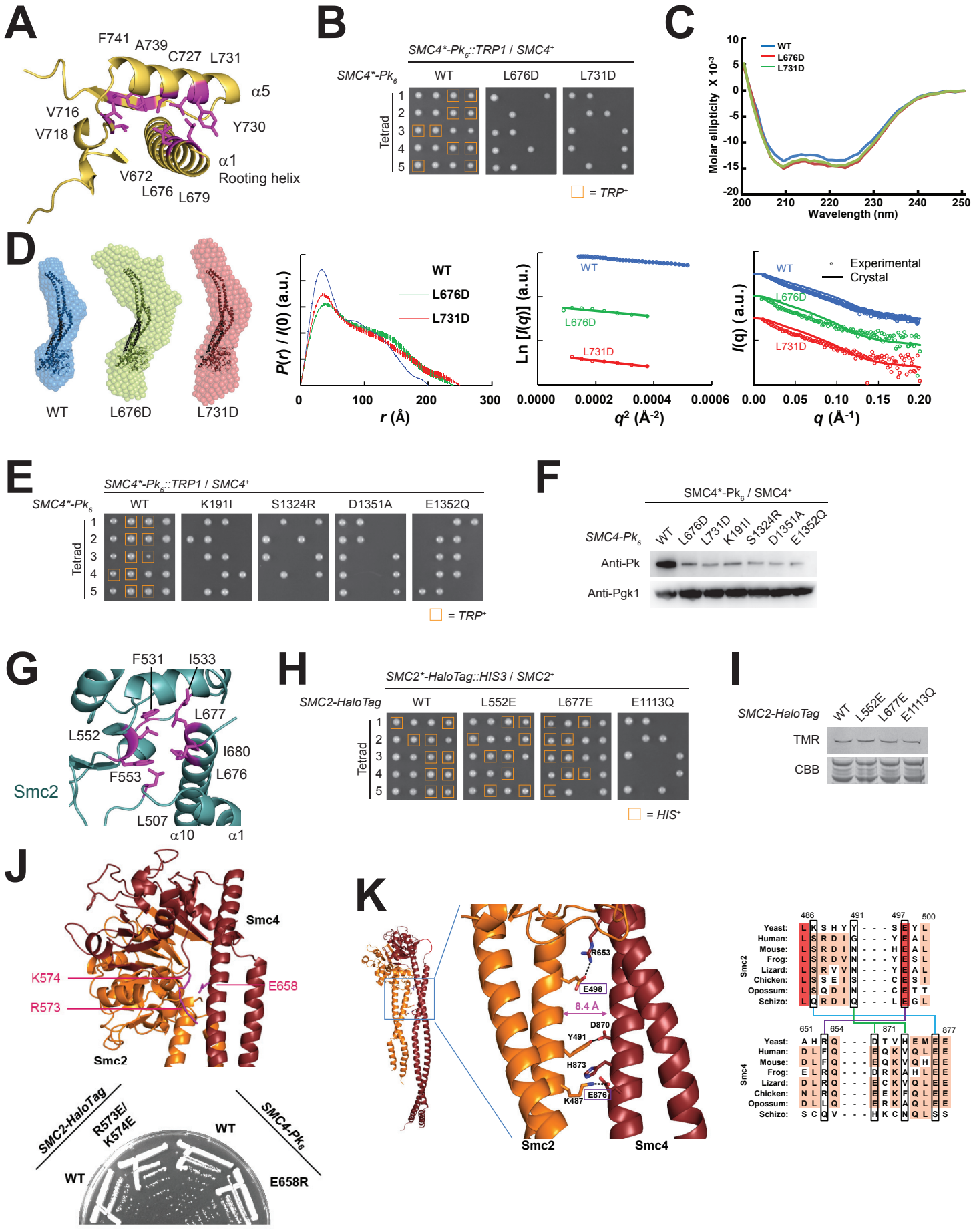

Figure S5

(Related to Figure 6)

Figure S5. Coils/coils and coils/hinge interactions at the yeast Smc2–4 condensin hinge. Related to Figure 6.

(A) Conserved residues at the Smc4 coils/hinge transition. Hydrophobic residues at the interface are display in stick representation in purple color. Same as Fig. 6C.

(B) Mutations in conserved residues on the Smc4 rooting helix are lethal in yeast. Tetrad dissection analysis of diploid yeast strains heterozygous for SMC4 genes. Spores of five tetrads were outgrown on YPAD at 30 °C and segregation of the modified alleles was monitored by testing for tryptophan prototrophy (orange box). Yeast strains: YSG079, YSG163 and YSG164.

(C) CD spectra of wild-type and mutant *Sc*Smc2H-CC110–*Sc*Smc4H-CC110 complexes.

(D) Dummy atom models for wild-type and mutant *Sc*Smc2H-CC110–*Sc*Smc4H-CC110 complexes based on SAXS measurements. The overall shapes of the mutant complexes are similar to the wild type but slightly more extended. *P(r)* graphs, Guinier plots and SAXS curves are shown. The discrepancies (χ^2) between the experimental *I*(*q*) curves and the theoretical *I*(*q*) curve calculated from the crystal structure of *Sc*Smc2H-CC110–*Sc*Smc4H-CC110 are WT = 32.16, L676D = 9.71, L731D = 10.36. Please note that the crystal structure of *Sc*Smc2H-CC110–*Sc*Smc4H-CC110 (PDB entry: 4RSI) contains only about half of the Smc2 coiled coil present in the *Sc*Smc2H-CC110–*Sc*Smc4H-CC110 construct.

(E) Smc4 ATPase mutations are lethal in yeast. As in (B), but SMC4-Pk$_6$ ATPase mutants were tested. K191I and D1351A block ATP binding, S1324R blocks head engagement, E1352Q blocks ATP hydrolysis. Yeast strains: YSG079, YSG172, YSG173, YSG174 and YSG175 (left).

(F) Smc4 mutant proteins are poorly expressed in yeast. Immunoblot analysis of strains shown in (B) and (E). The membrane was probed for Smc4-Pk$_6$ and Pgk1 as a loading control.

(G) Conserved residues at the Smc2 coils/hinge transition. Hydrophobic residues at the interface are display in stick representation in purple color. Same image as Figure 6C.

(H) Mutations at the Smc2 coils/hinge interface are not lethal. Tetrad dissection analysis of diploid yeast strains heterozygous for SMC2-HaloTag genes. Spores of tetrads were outgrown on YPAD at 30 °C and segregation of the modified alleles was monitored by testing for histidine prototrophy (orange box). Only the ATP hydrolysis defective Smc2(E1173Q) mutant is lethal. Yeast strains: YSG186-189.

(I) Smc2 mutant proteins are expressed at normal levels in yeast.
(J) Non-essential interactions between the Smc4 coiled coil and the Smc2 hinge domain. Contact between Arg573 and Lys574 in the Smc2 hinge and Glu658 on the Smc4 coiled coil (top). Yeast strains (YSG070, YSG143, YSG144 and YSG145) containing the charge reversal mutations, Smc2(R573E, K574E) and Smc4(E658R), were viable when grown on YPAD medium at 30 °C for 24 h (bottom).
(K) Interactions between Smc2 and Smc4 coiled coils. The interacting residues are shown in stick representation. The closest separation between the two helices is shown, which is much wider (>8 Å) than the ~5 Å separations in the *Pf* Smc (Fig 2C). Conserved residues (>80%) are indicated by rectangular boxes. The interacting pairs are linked by lines on the multiple sequence alignment. None of these exhibit obvious pairwise conservation.

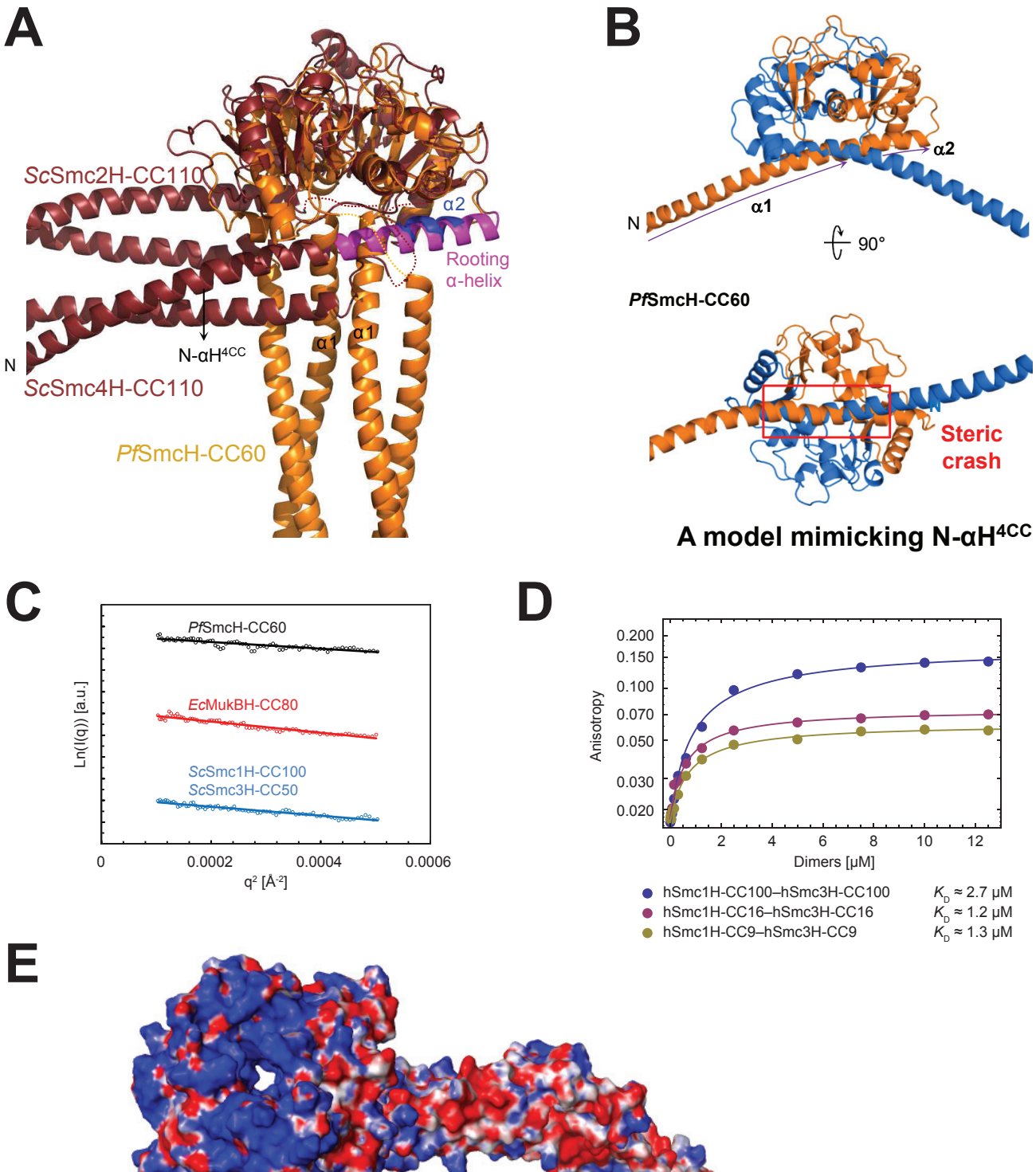

Figure S6

(Related to Figure 7)

Figure S6. Structural comparison of the symmetric and asymmetric coils/hinge organization in Smc–ScpAB and condensin. Related to Figure 7.

(A) Superimposition of the structures *Pf*SmcH-CC60 and *Sc*Smc2-CC110–*Sc*Smc4H-CC110 shows structural overlap of the rooting helix α2 in *Pf*SmcH-CC60 (displayed in blue color) with the rooting helix α1 in Smc4 (displayed in pink color).

(B) Modeling. The molecular symmetry prevents α1 and α2 of the *Pf* Smc hinge from forming a single continuous α-helix. The C-terminal coiled-coil helix is omitted for clarity.

(C) Guinier plots of the SAXS experiments shown in Figure 7.

(D) DNA binding of the human cohesin hinge with different lengths of coiled coil. Fluorescence anisotropy of fluorescein labeled DNA (40 bp) was measured.

(E) Electrostatic potential map of the *Sc*Smc2H-CC110–*Sc*Smc4H-CC110 dimer displayed from -6 k_BT/e (red) to +6 k_BT/e (blue).

SUPPLEMENTAL TABLES

Table S1. Genotypes of *Bacillus subtilis* strains

Name	Genotype
BSG1001	*Bacillus subtilis 1A700, trpC2*
BSG1007	*trpC2, Δsmc ftsY::ermB*
BSG1363	*trpC2, smcTmHinge ftsY::specR*
BSG1365	*trpC2, smcTmHinge(S535N) ftsY::specR*
BSG1366	*trpC2, smcTmHinge(A542T) ftsY::specR*
BSG1367	*trpC2, smcTmHinge(D518N) ftsY::specR*
BSG1368	*trpC2, smcTmHinge(N522D) ftsY::specR*
BSG1711	*trpC2, smc-tev-halotag ftsY::ermB*
BSG1760	*trpC2, smc(D491C)-tev-halotag ftsY::ermB*
BSG1761	*trpC2, smc(M492C)-tev-halotag ftsY::ermB*
BSG1762	*trpC2, smc(T495C)-tev-halotag ftsY::ermB*
BSG1763	*trpC2, smc(Q708C)-tev-halotag ftsY::ermB*
BSG1764	*trpC2, smc(K712C)-tev-halotag ftsY::ermB*
BSG1765	*trpC2, smc(A715C)-tev-halotag ftsY::ermB*
BSG1821	*trpC2, smc(D716C)-tev-halotag ftsY::ermB*
BSG1822	*trpC2, smc(E719C)-tev-halotag ftsY::ermB*
BSG1823	*trpC2, smc(E722C)-tev-halotag ftsY::ermB*
BSG1921	*trpC2, smc(C119S, C437S, A715C, C826S, C1114S)-tev-his-halotag (C61V, C262A) ftsY::ermB*
BSG1932	*trpC2, smc(C119S, C437S, TmHinge, A715C, C826S, C1114S)-tev-his-halotag (C61V, C262A) ftsY::ermB*
BSG1934	*trpC2, smc(C119S, C437S, TmHinge(S535N), A715C, C826S, C1114S)-tev-his-halotag(C61V, C262A) ftsY::ermB*
BSG1966	*trpC2, smcTmHinge(V664D) ftsY::ermB*
BSG1970	*trpC2, smcTmHinge(F665S) ftsY::ermB*

Table S2. Genotypes of yeast strains

Name	Genotype
YSG006	*Saccharomyces cerevisiae* W303, MATa
YSG008	*Saccharomyces cerevisiae* W303, MATa/α
YSG070	W303, MATa, SMC4-Pk6::TRP1
YSG079	W303, MATa/α, SMC4/SMC4-Pk6::TRP1
YSG081	W303, MATa, SMC2-HaloTag::HIS3, SMC4-Pk6::TRP1
YSG099	W303, MATa, SMC2(N506C)-HaloTag::HIS3, SMC4(Q654C)-Pk6::TRP1
YSG100	W303, MATa, SMC2(C494S, E498C)-HaloTag::HIS3, SMC4(E862C)-Pk6::TRP1
YSG101	W303, MATa, SMC2(C494S, K495C)-HaloTag::HIS3, SMC4(R866C)-Pk6::TRP1
YSG102	W303, MATa, SMC2(K487C, C494S)-HaloTag::HIS3, SMC4(E876C)-Pk6::TRP1
YSG143	W303, MATa, SMC2(R573E, K574E)-HaloTag::HIS3
YSG144	W303, MATa, SMC4(E658R)-Pk6::TRP1
YSG145	W303, MATa, SMC2-HaloTag::HIS3
YSG158	W303, MATa, SMC2(K487C, C494S)-HaloTag::HIS3, SMC4(Q654C)-Pk6::TRP1
YSG163	W303, MATa/α, SMC4(L676D)-Pk6::TRP1/SMC4
YSG164	W303, MATa/α, SMC4(L731D)-Pk6::TRP1/SMC4
YSG172	W303, MATa/α, SMC4(K191I)-Pk6::TRP1/SMC4
YSG173	W303, MATa/α, SMC4(S1324R)-Pk6::TRP1/SMC4
YSG174	W303, MATa/α, SMC4(D1341A)-Pk6::TRP1/SMC4
YSG175	W303, MATa/α, SMC4(E1352Q)-Pk6::TRP1/SMC4
YSG186	W303, MATa/α, SMC2-HaloTag::HIS3/SMC2
YSG187	W303, MATa/α, SMC2(L552E)-HaloTag::HIS3/SMC2
YSG188	W303, MATa/α, SMC2(L677E)-HaloTag::HIS3/SMC2
YSG189	W303, MATa/α, SMC2(E1113Q)-HaloTag::HIS3/SMC2
YSG192	W303, MATa, SMC2(C494S, Q681C)-HaloTag::HIS3, SMC4(Q654C)-Pk6::TRP1
YSG193	W303, MATa, SMC2(C494S, Q685C)-HaloTag::HIS3, SMC4(E862C)-Pk6::TRP1
YSG194	W303, MATa, SMC2(C494S, K688C)-HaloTag::HIS3, SMC4(R866C)-Pk6::TRP1

Table S3. SAXS derived parameters. Related to Figures 7.

Proteins	R_g (Å)	D_{max} (Å)	$Mass_{SAXS}$ (kDa)	$Mass_{Sequence}$ (kDa)
*Pf*SmcH-CC60	40 ± 1	134	58.9	61.6
*Ec*MukH-CC80	68 ± 1	239	68.3	68.1
*Sc*Smc1H-CC100–*Sc*Smc3H-CC50	56 ± 1	185	71.8	77.0
*Sc*Smc2H-CC110–*Sc*Smc4H-CC110	59 ± 1	200	104	90.5
*Sc*Smc2H-CC110–*Sc*Smc4H-CC110(L676D)	68 ± 4	240	125	90.5
*Sc*Smc2H-CC110–*Sc*Smc4H-CC110(L671D)	68 ± 4	250	113	90.5

The radius of gyration (R_g) was derived from the equation $I(q)= I(0) \exp(-q^2R_g^2/3)$; the maximum diameter ($D_{max}$) from $P(r)$; molecular mass from the absolute $I(0)$ intensity or from the scattering curve ($q< 0.2$) based on Q_R ($Mass_{SAXS}$) (Rambo and Tainer, 2013). R_g, D_{max} and $Mass_{SAXS}$ of *Sc*Smc2H-CC110–*Sc*Smc4H-CC110 (WT) were calculated from the $I(q)$ curve extrapolated to infinite dilution. Those of mutants were calculated from the $I(q)$ curve at one protein concentration: 1 mg/mL (L676D) and 1.2 mg/mL (L731D). The experimental *I(q)* curve of *Pf*SmcH-CC60, *Ec*MukBH-CC80 and *Sc*Smc1H-CC100–*Sc*Smc3H-CC100 were measured at 4.0, 6.0 and 1.9 mg/mL, respectively.

SUPPLEMENTAL EXPERIMENTAL PROCEDURES

Purification of *Pf*SmcH-CC60

The DNA fragment encoding *P. furiosus* Smc residues 445-720 was ligated into pET-22b-CPD 10H, a modified pET-22b plasmid (Novagen) to express target protein with a C-terminal fusion of a His_{10}-tagged cysteinyl protease domain (CPD) derived from *Vibrio cholerae* (Shen et al., 2009). Each of the two proteins was expressed in *E. coli* BL21(DE3) RIPL strain (Novagen). Cell lysate prepared in Buffer A was heat treated in a 80 ^{o}C water bath for 30 min. The resulting supernatant was loaded onto a column containing HisPur^{TM} Co resin, and the resin was equilibrated with Buffer A containing additional 1 mM inositol hexakisphosphate for 1 h at 4 ^{o}C to cleave off the CPD-$(His)_{10}$ tag. *Pf*SmcH-CC60 was further purified using a Hitrap Q column and a HiLoad 26/60 Superdex 200 column.

Purification of *Sc*Smc2H-CC110–*Sc*Smc4H-CC110

The DNA fragments encoding yeast Smc2 residues 396-792 and yeast Smc4 residues 555-951 were inserted into a modified pRSFDuet-1 vector by standard PCR-based cloning methods. *Sc*Smc2H-CC110 with an N-terminal $(His)_{10}$-tag and *Sc*Smc4H-CC110 without a tag were co-expressed in the *E. coli* BL21(DE3) RIPL strain (Novagen). Cell lysate was applied onto a gravity flow column containing HisPur^{TM} Cobalt Resin (Thermo Scientific). The column was washed with Buffer A containing 20 mM Tris-HCl (pH 7.5), 0.1 *M* NaCl and 3 mM β-mercaptoethanol (β-ME), and the complex was eluted with Buffer A containing additional 150 m*M* imidazole. After TEV protease treatment overnight the complex was further purified using a Hitrap Q anion exchange column (GE Healthcare) and HiLoad 26/60 Superdex 200 gel filtration column (GE Healthcare). Initially, selenomethionine (SelMet) was incorporated into both proteins, but the resulting complex yielded only poorly diffracting crystals. Subsequently, SelMet was incorporated only into *Sc*Smc4H-CC110. For separate production of the two proteins, the DNA fragment encoding *Sc*Smc4H-CC110 was cloned into pET-30a (Novagen) and that encoding *Sc*Smc2H-CC110 into pProExHTa (Invitrogen). SelMet-substituted *Sc*Smc4H-CC110 was expressed in *E.coli* B834(DE3) RIL (Novagen), and native *Sc*Smc2H-CC110 was expressed in *E. coli* BL21(DE3) RIPL strain. The cells obtained from the two different

cultures were co-sonicated, and the half labeled SelMet-complex was purified in the same way as the native protein complex.

Purification of *Bs*SmcH-CC100

The DNA fragment encoding *B. subtilis* Smc residues 400-776 was ligated into the pET-22b-CPD 10H vector. The protein was expressed in the *E. coli* BL21 (DE3) RIPL strain at 18 ^{o}C. Bacterial cell lysate was prepared by sonication in Buffer A and loaded onto a column containing HisPur^{TM} Co resin (Thermo Scientific). After on-gel digestion reaction with 1 mM inositol hexakisphosphate to cleave off the CPD-$(His)_{10}$ tag, *Bs*SmcH-CC100 was further purified using a HitrapQ column and a HiLoad 26/60 Superdex 200 gel-filtration column. The final sample was concentrated up to 20 mg/ml using a Amicon Ultra centrifugal filter.

Purification of *B. subtilis* Smc–ScpAB

The DNA fragment encoding *B. subtilis* Smc was ligated into pET-22b, and those encoding ScpA and ScpB into a modified pRSF Duet vector. The three proteins were coexpressed in the *E. coli* BL21(DE3) strain at 18 ^{o}C. Bacterial cell lysate was prepared by sonication in Buffer A with 0.35 M NaCl and loaded onto a column containing HisPur^{TM} Co resin. The column was equilibrated with Buffer A with 0.35 M NaCl and 1 mM inositol hexakisphosphate for 1 h at 4 ^{o}C to cleave off the CPD-$(His)_{10}$ tag. The complex was further purified using a Hitrap Q anion exchange column and HiLoad 26/60 Superdex 200 gel filtration column. The final buffer contained 20 mM HEPES pH 7.5, 0.35 M NaCl, 10% Glycerol, 1 mM EDTA, and 1 mM DTT.

Purification of *B. subtilis* Smc and Smc(A715C)

Wild-type *Bs* Smc and cysless Smc(A715C) protein was expressed and purified as described in (Fuentes-Perez et al., 2012) with an additional Superose 6 10/300 GL (GE Healthcare) gel filtration added as a final step in the purification. Gel filtration was performed in storage buffer 50 mM Tris-HCl at pH 7.5, 150 mM NaCl, and 1 mM DTT.

Purification of *Bs*SmcH

*Bs*SmcH (residues 498-665) was cloned into pET-22b. Expression was performed in

Escherichia coli BL21 (DE3) Gold for 14 hr at 27 °C. The full-length Smc protocol was followed for the first Blue Sepharose FF column (GE Healthcare). Peak fractions were then run on Superdex 200 10/300 GL gel filtration (GE Healthcare) in storage buffer.

Purification of *Bs*SmcH-CC8-His6

The *Bs* Smc hinge with short coiled coils (residues 489-680) was fused to a C-terminal HISx6-CYS tag and cloned into pET-28 (to yield plasmid pSG1530). The protein was expressed in *E. coli* BL21 (DE3) Gold in auto-induction medium (overnight express TB broth, Novagen) at 25°C for 24 hr and purified in two steps via a HisTrap column (GE Healthcare) and by gel filtration (Superdex 200 10/300 GL) into storage buffer.

Purification of His6-*Bs*SmcH-CC100 for cross-linking analysis

His6-*Bs*SmcH-CC100 constructs containing the C437S mutation were produced from pET-28 derived vectors in *E. coli* BL21-Gold (DE3) for 24 h at 24 °C using auto-induction medium (OvernightExpress TB, Novagen). Extracts were prepared by sonication in 50 mM NaPi, pH 7.4 / 4 °C, 300 mM NaCl, 80 mM imidazole, 10 % glycerol, 1 mM DTT and bound to Ni^{2+} Sepharose FF (GE Healthcare). Columns were washed with 10 column volumes (CV) of binding buffer, followed by 5 CV of 50 mM NaPi, pH 7.4 / 4 °C, 1 M NaCl, 10 % glycerol, 1 mM DTT, followed by 5 CV of binding buffer. Proteins were eluted with 500 mM imidazole, pH 7.4 / 4 °C, 300 mM NaCl, 10 % glycerol, 1 mM DTT and further purified on Superdex 200 in 50 mM Tris-HCl, 200 mM NaCl, 1 mM TCEP, pH 7.4 / 4 °C (final). Aliquots were flash frozen in liquid N_2 and stored at -80 °C.

Purification of *Bs*SmcH-CC300

*Bs*SmcH-CC300 (residues 188-1011) with an N-terminal His-TEVs tag was purified under similar conditions as His6-*Bs*SmcH-CC100, except that an additional TEV protease cleavage step was included.

Purification of *Ec*MukBH-CC80

The DNA fragment encoding *E. coli* MukB residues 566-863 was ligated into a modified pProEx HTa vector containing a $(His)_{10}$ tag. The protein was expressed in the *E. coli* BL21 (DE3) strain at 18 °C. Bacterial cell lysate was prepared by sonication in Buffer

containing 20 mM Tris-HCl (pH 7.5), 0.45 M NaCl and 3 mM β-ME, and loaded onto a column containing HisPur^{TM} Co resin. The protein was eluted with Buffer A containing additional 150 mM imidazole. After TEV protease treatment overnight, the protein was further purified using a Hitrap Q anion exchange column and HiLoad 26/60 Superdex 200 gel filtration column. The *Ec*MukBH-CC80 variant containing a C730A mutation, which was used for FRET analysis, was expressed and purified in the same manner as the wild-type version of the protein.

Purification of *Sc*Smc1H-CC100 and *Sc*Smc3H-CC50

The DNA fragments encoding yeast Smc1 residues 399-794 and Smc3 residues 467-743 were ligated into a pET-30a (Novagen) and pProExHTa (Invitrogen) vector, respectively. The two proteins were co-expressed in the *E. coli* BL21 (DE3) RIPL codon plus strain at 18 ^{o}C. The protein complex was purified in the same manner as *Sc*Smc2H-CC110–*Sc*Smc4H-CC110.

Purification of human Smc1–3 hinge complexes

The DNA fragments encoding human Smc1 residues 499-675, 471-685 or 382-784 were ligated into the pET-30a vector. The DNA fragments encoding Smc3 residues 492-685, 484-696 or residues 400-774 were ligated into the pProExHTa vector. Three pairs of the proteins, Smc1(499-675) and Smc3(492-685) (=hSmc1H-CC9–Smc3H-CC9), Smc1(471-685) and Smc3(484-696) (=hSmc1H-CC16–hSmc3H-CC16) and Smc1(382-784) and Smc3(400-774) (=hSmc1H-CC100–hSmc3H-CC100), were co-expressed in the *E. coli* BL21 (DE3) RIPL strain at 18 °C. The protein complexes were purified in the same manner as *Sc*Smc2H-CC110–*Sc*Smc4HCC110.

Crystallization, X-ray data collection and structure determination

Initial crystals of *Pf*SmcH-CC60 (40 mg/ml) were obtained by the sitting-drop vapor-diffusion method at 22 °C in a precipitant solution containing 1 M sodium citrate and 0.2 M CHES (pH 9.5). Larger single crystals were grown by the hanging-drop vapor-diffusion method at 22 °C from a precipitant solution containing 1 M sodium citrate, 0.1 M CHES (pH 9.5) and 8% glycerol. The *Sc*Smc2H-CC110–*Sc*Smc4H-CC110 complex (20 mg/ml) was crystallized using the hanging-drop vapor diffusion technique at 20 °C in a

precipitant solution containing 16% PEG 300, 0.1 *M* Na/K phosphate pH 6.0, 8% glycerol and 10 m*M* dithiothreitol (DTT). The SelMet-substituted complex was crystallized under the same crystallization condition. X-ray diffraction data were collected at the beamline BL17A at the Photon Factory, Japan and the beamline 5C at the Pohang Accelerator Laboratory, Korea. A native data set was collected for *Pf*SmcH-CC60. A single-wavelength anomalous dispersion (SAD) data set was collected with a SelMet-substituted *Sc*Smc2H-CC110–*Sc*Smc4H-CC110 crystal at the Se absorption peak. Obtaining good data set for the *Sc*Smc2H-CC110–*Sc*Smc4H-CC110 crystal was exhausting at its thin crystal easily bent due to minor crystal contacts in one direction. All diffraction data were processed with HKL2000 (Otwinowski and Minor, 1997). The structure of *Pf*SmcH-CC60 was determined by molecular replacement using the structure of the coiled coil-less *Pf* Smc hinge (PDB entry: 3NWC) as a probe by using the program Phenix AutoMR (McCoy et al., 2007). The *Sc*Smc2H-CC110–*Sc*Smc4H-CC110 structure was solved by the single isormorphous replacement with anomalous scattering (SIR-AS) method. The model building and structure refinement were carried out using the programs *COOT* (Emsley and Cowtan, 2004) and *CNS* (Brunger et al., 1998). The final model of *Sc*Smc2H-CC110–*Sc*Smc4H-CC110 does not include residues 671-673 of Smc2 and 836-841 of Smc4, which are disordered in the crystals. Crystallographic data statistics are summarized in Table 1.

SAXS analysis

SAXS data were collected on the BL45XU beamline SPring8 (for *Sc*Smc2H-CC110–*Sc*Smc4H-CC110) and a BioSAXS-1000 system (for mutants thereof) and on the 4C SAXS II beamline at Pohang Light Source II (for *Pf*SmcH-CC60, *Ec*MukBH-CC80 and *Sc*Smc1H-CC100–*Sc*Smc3H-CC50). The PILATUS300k-w detector on the BL45XU beamline, at a sample-to-detector distance of 3496 mm, was used to measure scattering intensities at 20 °C. The SX165 detector on the 4C SAXS II beamline, at a sample-to-detector distance of 2000 or 4000 mm, was used to measure scattering intensities at 4 °C. Samples of varying protein concentrations were used to obtain triplicate measurements per each sample with an exposure time 30 to 60 sec at 0.675 Å or 1.000 Å wavelength. The data were processed and analyzed using the software applications embedded in the ATSAS package [http://www.embl-hamburg.de/biosaxs/software.html].

The one-dimensional scattering data $I(q)$ as a function of q ($q = 4\pi\sin\theta/\lambda$, where 2θ is the scattering angle and λ is the wavelength) was obtained through radial averaging. Scattering intensities from the buffer solution were measured and used for background subtraction. The $I(q)$ data of the samples were then extrapolated to zero concentration. The program GNOM was used to calculate the distance distribution function $P(r)$. The maximum dimension (D_{max}) of the particle, was determined from the $P(r)$ function, the distance r where $P(r) = 0$. Molecular envelope models were produced by program DAMMIF (Franke and Svergun, 2009). Six independently calculated, low-resolution dummy atom models were averaged by program DAMAVER (Volkov and Svergun, 2003). Superposition of the molecular envelopes and crystal structures was carried out by program SUPCOMB (Kozin and Svergun, 2001). SAXS data for the *Sc*Smc2H-CC110–*Sc*Smc4H-CC110 mutants were collected with BioSAXS-1000 (Rigaku) mounted on a MicroMax007HF X-ray generator (Rigaku). The PILATUS100k detector, at a sample-to-detector distance 484 mm, was used to measure scattering intensities at 20 °C. The protein concentration was 1 mg/mL and 1.2 mg/mL for the L676D and the L731D mutant, respectively. Quadruple measurements were obtained per each sample with 1 h exposure at 1.5418 Å wavelength.

ALEX-FRET and TIRF-FRET analyses

The BsSmcH-CC100 homodimer was labeled with Cy3- and Cy5-maleimide (GE Healthcare). For dual labeling, the two fluorescent dyes were added at a 1:2 (protein:dye) molar ratio. The mixture was incubated for 6 h at 4 ^{o}C. Unreacted dyes were removed by a PD minitrap G-25 size-exclusion column (GE healthcare). The dye labeling was confirmed by a fluorescent protein band on a SDS-PAGE gel. The reaction mixture containing three types of products, Cy3-BsSmcH-CC100-Cy3 (donor only), Cy5-BsSmcH-CC100-Cy5 (acceptor only) in addition to Cy3-BsSmcH-CC100-Cy5 (FRET pair), was used for single-molecule techniques. The ALEX-FRET method and data analysis were described in previous works (Kim et al., 2012; Lee et al., 2005). The laser intensities for donor and acceptor excitation were 80 μW and 35 μW, respectively. In order to detect single-diffusing molecule in solution, the protein sample was diluted approximately to 50 pM in a buffer solution containing 20 mM Tris-HCl (pH 7.5), 100 mM NaCl, 1 mM NaN_3, 1 mM DTT, 5% glycerol (v/v), 100 μg/ml bovine serum albumin and 1 mM β-ME. The LABVIEW software (National

Instrument) was used to select fluorescent bursts induced by single molecules. The FRET efficiency (E) and stoichiometry parameter (S) were calculated as described previously (Lee et al., 2005):

$$E = \frac{I_D^A}{I_D^D + I_D^A}, \quad S = \frac{I_D^D + I_D^A}{I_D^D + I_D^A + I_A^A},$$

where I_D^A (D: donor, A: acceptor) denotes a fluorescent emission of acceptor dye by donor excitation (FRET signal), I_D^D a fluorescent emission of donor dye excited by donor-excitation laser, I_A^A a fluorescent emission of acceptor dye excited by acceptor-excitation laser. The noises were corrected that arise from the leakage (donor emission detected by acceptor detector), the direct acceptor excitation and the intrinsic noise of laser scattering. The ratio of detection efficiency was ~1. The distance between Cy3 and Cy5 was estimated by the equation of $R = R_0(1/E-1)^{1/6}$ with the R_0 value of 6 nm for the Cy3-Cy5 pair (Roy et al., 2008).

For TIRF-FRET analysis, dye-labeled BsSmcH-CC100 was first encapsulated in a lipid vesicle. Synthetic lipids, 1-palmitoyl-2-oleoyl-sn-glycero-3-phosphocholine, 1,2-dioleoyl-sn-glycero-3-[phospho-L-serine], cholesterol, 1-palmitoyl-2-oleoyl-sn-glycero-3-phophoethanolamine and 1,2-Dipalmitoyl-sn-Glycero-3-phosphoethanolamine-N-Biotinyl, were purchased from Avanti Polar Lipids and mixed with molar ratios of 64.9:5:20:10:0.1. After forming large unilamellar vesicles (Kim et al., 2012), extrusion using mini extruder (Avanti Polar Lipids) with 100 nm polycarbonate filter (Whatman) was performed to make mono-disperse unilamellar vesicles. During this process, dye-labeled BsSmcH-CC100 was added for encapsulation inside a vesicle. To ensure one or less than one protein molecule per vesicle for single-molecule detection, the molar ratio of the protein and vesicle was kept approximately 1:100. Unencapsulated protein was removed by a CL-4b column (Sigma). The vesicles were attached onto a quartz glass coated with PEG-biotin and PEG (1:40 mass ratio, Laysan Bio) via Neutravidin (PIERCE). To increase photostability, the flow chamber was washed at each step with an oxygen scavenger buffer containing 20 mM Tris-HCl (pH 7.5), 100 mM NaCl, 1 mM NaN_3 and 1 mM DTT. A prism type TIRF setup based on an inverted microscope (IX71, Olympus) with water-immersion objective (60X, 1.20 NA, UPlanSApo, Olympus) was used for real-time observation. The power of the donor excitation laser (532 nm laser, Cobolt) was

50 μW. The fluorescent emission from the sample was separated into two pathways depending on the wavelength by dual viewer (DV2, Photometrics). A dichroic mirror (FF624, Semrock) was used for dividing donor and acceptor emissions, which were filtered by FF01-580/60 (Semrock) and FF01-675/67 (Semrock), respectively. The images were recorded using an EMCCD (Andor DU-897D) with a 10 frames/sec acquisition speed. The ratio of the detection efficiency (acceptor detection efficiency/donor detection efficiency) was ~1.2 in the TIRF-FRET system. A fluorescence time trace showed a clear one-step acceptor beaching, followed by a donor bleaching, which ensured encapsulation of a single molecule per vesicle.

Anisotropy Titration Measurements.

Fluorescence anisotropy titrations were performed at 25 °C using a BioTek Neo plate reader in a buffer containing 50 mM Tris-HCl at pH 7.5, 50 mM NaCl, and 2-3 mM $MgCl_2$ (+ 1 mM ATP). Anisotropy was measured with the instrument in the T format, allowing simultaneous acquisition of parallel (I//) and perpendicular (I⊥) components. Anisotropy was calculated based upon (Brownbridge et al., 1993).

Total fluorescence intensity (F_t) is given by:

$$F_t = \sum c_i F_i$$

Total anisotropy (A_t) is given by:

$$A_t = \frac{\sum c_i F_i A_i}{F_t}$$

Where c_i is the concentration of species i, F_i is the fluorescence intensity per unit of concentration and A_i is the anisotropy. This is calculated from the parallel and perpendicular fluorescence intensity (I) in relation to the plane of excitation by:

$$A_i = \frac{I_{parallel} - I_{perpendicular}}{I_{parallel} + 2I_{perpendicular}}$$

As anisotropy is additive for multiple fluorescence species in solution, it is used to give a measure of their relative concentrations. For Smc (and various constructs) there are two fluorescence species, DNA and Smc.DNA. The total anisotropy can then be calculated in terms of the dissociation constant (K_D) for the Smc.DNA complex:

$$A_t = \frac{A_{DNA}([DNA]_t - [Smc.DNA]) + A_{Smc.DNA}Q[Smc.DNA]}{[DNA]_t - [Smc.DNA] + Q[Smc.DNA]}$$

Where

$$[Smc.DNA] = \frac{([Smc]_t + [DNA]_t + K_D) - \sqrt{([Smc]_t + [DNA]_t + K_D)^2 - 4[Smc]_t[DNA]_t}}{2}$$

And where $[Smc]_t$ and $[DNA]_t$ are the total concentrations for each reactant. [Smc.DNA] is the concentration of the protein-bound DNA complex. Q is the fluorescence intensity of Smc.DNA relative to DNA. The anisotropy data were fitted to obtain dissociation constants based on the above equations using GraFit fitting software (Leatherbarrow, 2001).

DNA Substrates

Labeled and unlabeled oligonucleotides were purchased from Sigma-Aldrich. To form DNA substrates, oligonucleotides were mixed at equimolar concentrations at 50 µM in either water or a buffer containing 50 mM Tris-HCl at pH 7.5, 150 mM NaCl, and 3 mM $MgCl_2$.

ds40 A TTAGTTGTTCGTAGTGCTCGTCTGGCTCTGGATTACCCGC*
ds40 B GCGGGTAATCCAGAGCCAGACGAGCACTACGAACAACTAA
*is fluorescein

Dynamic light scattering

*Bs*SmcH-CC100(C437S, A715C) protein (6.5 µM) was incubated in 50 mM Tris-HCl, 50 mM NaCl, 2 mM $MgCl_2$, 0.25 mM TCEP, pH 7.5 (final) in the presence or absence of 20 µM DNA (40 bp). Measurements were performed at 20 °C in a DynaPro NanoStar instrument (Wyatt Technologies), analysed with DYNAMICS V7 (Wyatt Technologies) and results from multiple acquisitions were averaged. Mass distributions are shown assuming isotropic spheres.

Cysteine cross-linking and labeling of *Bs*SmcH-CC100

Protein and double stranded oligonucleotides (40 bp) were mixed at 4 µM and 20 µM, respectively, in 50 mM Tris-HCl, 50 mM NaCl, 2 mM $MgCl_2$, 0.25 mM TCEP, pH 7.5 / 23

°C (final). After incubation at room temperature for 5 min, BMOE was added to a final concentration of 0.5 mM from a 20 mM stock solution in DMSO. BM-dPEG$_n$ cross-linkers (Celares GmbH) and Oregon-Green maleimide (Life Technologies) were used at the same concentration. When no maleimide compound was used, an equal volume of DMSO was added. Reactions were incubated for 1 min at room temperature and quenched with 2-mercaptoethanol (14 mM).

Circular dichroism spectroscopy

Data were collected on a JASCO model J-810 spectropolarimeter with a 0.2 cm cuvette. CD spectrum was recorded over the range of 200–250 nm in a nitrogen atmosphere with the *Sc*Smc2H-CC110–*Sc*Smc4H-CC110 protein samples (0.1 mg/ml) dissolved in 40 mM sodium phosphate buffer (pH 7.0) containing 1 mM DTT. The spectrum was the accumulation of three scans corrected by subtracting signals from the buffer control.

Yeast strain construction

Yeast strains are derivatives of *Saccharomyces cerevisiae* W303. Genetic modifications of *SMC2* and *SMC4* loci were done by double crossover recombination. Mutants were selected on synthetic media and maintained on YPAD after single colony purification. Genotypes are listed in Table S2.

Immunoprecipitation and cysteine cross-linking

Yeast was diluted from a stationary phase overnight culture into fresh YPAD to an A_{600} of 0.1. Cells were grown at 30 °C to an A_{600} of approximately 0.8 and harvested by centrifugation, washed in ice cold PBS and snap frozen in PBS supplemented with a protease inhibitor cocktail (Sigma). A concentrated buffer solution was added to each pellet adjusting the conditions to 85 mM sodium phosphate (pH 7.4), 120 mM NaCl, 1 mM EDTA and 14 mM β-ME. Frozen material was broken in a swing mill, quickly thawed and centrifuged for 2 x 10 min at 21,000 x g. The protein extract was incubated for 30 min at 4 °C with Dynabeads Protein G (Life Technologies) charged with monoclonal SV5-Pk1 antibody (AbD Serotec). Beads were washed twice in ice cold PBS, then resuspended in PBS. BMOE was added to a final concentration of 0.5 mM from a 20 mM stock solution in DMSO. When no cross-linker was used, an equal amount of DMSO was

added. Reactions were incubated for 10 min on ice before quenching with 2-ME at a final concentration of 14 mM. Beads were incubated for 15 min at 37 °C in PBS supplemented with protease inhibitors and 5 µM HaloTag TMR substrate (Promega) before boiling in SDS-PAGE sample buffer. Gels were analyzed on a Typhoon scanner (GE Healthcare) with Cy3 DIGE setup.

Immunoblot analysis

Yeast was grown as described above, washed once in PBS and then resuspended in 10 % (w/v) trichloroacetic acid followed by mechanical cell lysis and collection of precipitated protein by centrifugation. Electroblots were probed with SV5-Pk1 antibodies at a dilution of 1:2,000.

Construction of *Bs*Smc*Tm*H and suppressor mutagenesis

The chimeric Smc protein, *Bs*Smc*Tm*H, was constructed starting from a *Bs smc* targeting vector (pSG001) by replacing the *Bs smc* fragment encoding aa495-678 by the corresponding fragment of *Thermotoga maritima* MSB8 *smc*, aa491-670 (pSG1167). Random mutations in the *Tm* part of BsSmcTmH were generated by cloning of *Taq* polymerase amplified PCR products into the parental vector. A *smc* mutant lacking the hinge domain (BSG1306) was transformed with the cloned DNA library. Transformants were selected for growth on rich medium, *i.e.* nutrient agar, streaked for single colonies and characterized by PCR and sequencing. Selected mutations were cloned and re-transformed to ensure a clean genetic background.

Electrostatic surface potential for Smc hinge

A structural homology model for the *Bs* Smc hinge domain was generated based on the *Tm* Smc hinge coordinates (PDB: 1GXL) using Modeller software (Eswar et al., 2007) with default settings. Electrostatic surface potential maps were calculated using a APBS plugin in Pymol and displayed in Pymol at ± 6 kT/e (Baker et al., 2001).

SUPPLEMENTAL REFERENCES

Baker, N.A., Sept, D., Joseph, S., Holst, M.J., and McCammon, J.A. (2001). Electrostatics of nanosystems: application to microtubules and the ribosome. Proceedings of the National Academy of Sciences of the United States of America *98*, 10037-10041.

Brownbridge, G.G., Lowe, P.N., Moore, K.J., Skinner, R.H., and Webb, M.R. (1993). Interaction of GTPase activating proteins (GAPs) with p21ras measured by a novel fluorescence anisotropy method. Essential role of Arg-903 of GAP in activation of GTP hydrolysis on p21ras. The Journal of biological chemistry *268*, 10914-10919.

Brunger, A.T., Adams, P.D., Clore, G.M., DeLano, W.L., Gros, P., Grosse-Kunstleve, R.W., Jiang, J.-S., Kuszewski, J., Nilges, M., and Pannu, N.S. (1998). Crystallography & NMR system: A new software suite for macromolecular structure determination. Acta Crystallogr. D Biol. Crystallogr. *54*, 905-921.

Emsley, P., and Cowtan, K. (2004). Coot: model-building tools for molecular graphics. Acta Crystallogr. D Biol. Crystallogr. *60*, 2126-2132.

Eswar, N., Webb, B., Marti-Renom, M.A., Madhusudhan, M.S., Eramian, D., Shen, M.Y., Pieper, U., and Sali, A. (2007). Comparative protein structure modeling using MODELLER. Current protocols in protein science / editorial board, John E. Coligan ... [et al.] *Chapter 2*, Unit 2 9.

Franke, D., and Svergun, D.I. (2009). DAMMIF, a program for rapid ab-initio shape determination in small-angle scattering. J. Appl. Cryst. *42*, 342-346.

Fuentes-Perez, M.E., Gwynn, E.J., Dillingham, M.S., and Moreno-Herrero, F. (2012). Using DNA as a fiducial marker to study SMC complex interactions with the atomic force microscope. Biophysical journal *102*, 839-848.

Kim, J.-Y., Choi, B.-K., Choi, M.-G., Kim, S.-A., Lai, Y., Shin, Y.-K., and Lee, N.K. (2012). Solution single-vesicle assay reveals PIP2-mediated sequential actions of synaptotagmin-1 on SNAREs. EMBO J. *31*, 2144-2155.

Kozin, M.B., and Svergun, D.I. (2001). Automated matching of high-and low-resolution structural models. J. Appl. Cryst. *34*, 33-41.

Lee, N.K., Kapanidis, A.N., Wang, Y., Michalet, X., Mukhopadhyay, J., Ebright, R.H., and Weiss, S. (2005). Accurate FRET measurements within single diffusing biomolecules using alternating-laser excitation. Biophys. J. *88*, 2939-2953.

McCoy, A.J., Grosse-Kunstleve, R.W., Adams, P.D., Winn, M.D., Storoni, L.C., and Read, R.J. (2007). Phaser crystallographic software. J Appl Cryst *40*, 658-674.

Mitov, M.I., Greaser, M.L., and Campbell, K.S. (2009). GelBandFitter--a computer program for analysis of closely spaced electrophoretic and immunoblotted bands. Electrophoresis *30*, 848-851.

Otwinowski, Z., and Minor, W. (1997). Processing of X-ray diffraction data. Methods Enzymol. *276*, 307-326.

Rambo, R.P., and Tainer, J.A. (2013). Accurate assessment of mass, models and resolution by small-angle scattering. Nature *496*, 477-481.

Roy, R., Hohng, S., and Ha, T. (2008). A practical guide to single-molecule FRET. Nat. Methods *5*, 507-516.

Shen, A., Lupardus, P.J., Morell, M., Ponder, E.L., Sadaghiani, A.M., Garcia, K.C., and Bogyo, M. (2009). Simplified, enhanced protein purification using an inducible, autoprocessing enzyme tag. PloS one *4*, e8119.

Volkov, V.V., and Svergun, D.I. (2003). Uniqueness of ab initio shape determination in small-angle scattering. J. Appl. Cryst. *36*, 860-864.